nature biomedical engineering

ARTICLES

PUBLISHED: 13 JUNE 2017 | VOLUME: 1 | ARTICLE NUMBER: 0080

A fully functional drug-eluting joint implant

V. J. Suhardi[1,2,3], D. A. Bichara[1,2], S. J. J. Kwok[3,4], A. A. Freiberg[2], H. Rubash[2], H. Malchau[2], S. H. Yun[3,4], O. K. Muratoglu[1,2] and E. Oral[1,2]*

Despite advances in orthopaedic materials, the development of drug-eluting bone and joint implants that can sustain the delivery of the drug and maintain the necessary mechanical strength to withstand loading has remained elusive. Here, we demonstrate that modifying the eccentricity of drug clusters and the percolation threshold in ultra-high molecular weight polyethylene (UHMWPE) results in maximized drug elution and the retention of mechanical strength. The optimized UHMWPE eluted antibiotic at a higher concentration for longer than the clinical gold standard antibiotic-eluting bone cement, while retaining the mechanical and wear properties of clinically used UHMWPE joint prostheses. Treatment of lapine knees infected with *Staphylococcus aureus* with the antibiotic-eluting UHMWPE led to complete bacterial eradication and the absence of detectable systemic effects. We argue that the antibiotic-eluting UHMWPE joint implant is a promising candidate for clinical trials.

More than one million joint replacements are performed annually in the United States[1]. Five to ten percent of joint replacements are revised within seven years[2], with prosthetic joint infection (PJI) being one of the most common reasons for revision (Fig. KT29 in ref. [3]). PJI is an increasing healthcare burden[4] with a recurrence rate of 16% (ref. [5]) and a mortality rate of 2.5% (ref. [6]). End-stage treatments are severely morbid, including multiple revisions, resection arthroplasty, arthrodesis and amputation[7].

Antibiotic penetration into the joint space and bone from systemic administration is limited because of poor blood supply to the infected area[8]. A strategy to address this is to deliver antibiotics locally by incorporating them into orthopaedic implant materials[9,10]. The current treatments incorporate antibiotics into poly methyl-methacrylate bone cement[10], ceramic bone graft substitutes[11], or resorbable polymeric systems[12]. The gold standard in treating PJI involves two-stage surgery, where removal of all components of the infected implants is followed by a minimum of 6–8 weeks of antibiotic-eluting bone cement spacer placement, during which patients have limited mobility and function (Fig. 1)[13]. This period is followed by the placement of new implant components; however, in cases where the temporary spacers are used for long-term weight bearing without the placement of new implants, bone cement spacers have shown a complication rate of 26–60% within 49–54 months[14], mainly due to dislocation (11–17%) and fracture (10–14%). The primary use of bone cement in joint implants is fixation of the bone–implant interface; however, bone cement has low tensile strength and impact toughness[15,16] and is unsuitable for use in continuous load and articulation[17,18].

The high incidence of bone cement fractures (Fig. 1)[14] is also due to the decrease in mechanical properties caused by incorporated antibiotics[19]. In addition, although drug elution into the peri-prosthetic space is desired for 3–8 weeks, the elution from antibiotic-eluting bone cement spacers often falls below the minimum inhibitory concentration (MIC) of common PJI bacterial contaminants within 1 week[20]. Low antibiotic concentration without the complete eradication of bacteria has the potential of increasing antibiotic resistance[21]. The antibiotic concentration in bone cement is limited by the minimum allowed mechanical properties, but results in low interconnectivity of drug clusters (Fig. 1)[22]. In fact, for drug-eluting polymers with spherical drug clusters[23], 40–60% (w/w) drug content is required to reach complete interconnectivity. Our goal was to develop load-bearing joint implant materials with efficient antibiotic release for at least 3 weeks, and high mechanical strength and wear resistance within that of clinically used UHMWPE (Supplementary Discussion), to allow direct replacement of infected prosthetics with a new implant (Fig. 1) without the complications and morbidity associated with a two-stage procedure.

Drug cluster interconnectivity was studied using percolation theory, which showed that drug elution increased sharply as the percolation threshold was reached[24], whereas mechanical strength decreased with total drug content[25]. Computational simulation showed that increasing eccentricity of the drug cluster shape[26] and increasing polymer particle to drug cluster size ratio[27] may increase drug cluster interconnectivity. We hypothesized that by increasing the eccentricity of the drug clusters and increasing the polymer particle to drug cluster size ratio in a drug-incorporated polymer matrix, interconnectivity of drug clusters could be reached at lower drug content, thus improving the mechanical properties of the polymer matrix. We demonstrate application of this concept to UHMWPE to develop a load-bearing implant for the treatment of PJI.

Effect of cluster eccentricity on elution and strength

A comparison of drug elution rate and tensile mechanical properties was made for low density polyethylene (LDPE), which could be prepared using solvent casting, resulting in conventional spherical drug clusters (Fig. 2a,g; continuous) and compression moulding, resulting in highly eccentric drug clusters (Fig. 2a,g; highly eccentric). Variation in the content of the antibiotic drug vancomycin (2, 6 and 10 wt%) and the LDPE/vancomycin particle size ratio (6:1, 16:1, and 40:1) showed that the polymer with the highly eccentric drug clusters had a higher elution rate than the one with spherical drug clusters for 6 and 10 wt% drug loading (Fig. 2d–f). This

[1]Harris Orthopaedic Laboratory, Massachusetts General Hospital, Boston, Massachusetts 02114, USA. [2]Department of Orthopaedic Surgery, Harvard Medical School, Boston, Massachusetts 02115, USA. [3]Department of Medical Engineering and Medical Physics, Massachusetts Institute of Technology, Cambridge, Massachusetts 02139, USA. [4]Wellmann Center for Photomedicine, Massachusetts General Hospital, Boston, Massachusetts 02114, USA. *e-mail: eoral@partners.org

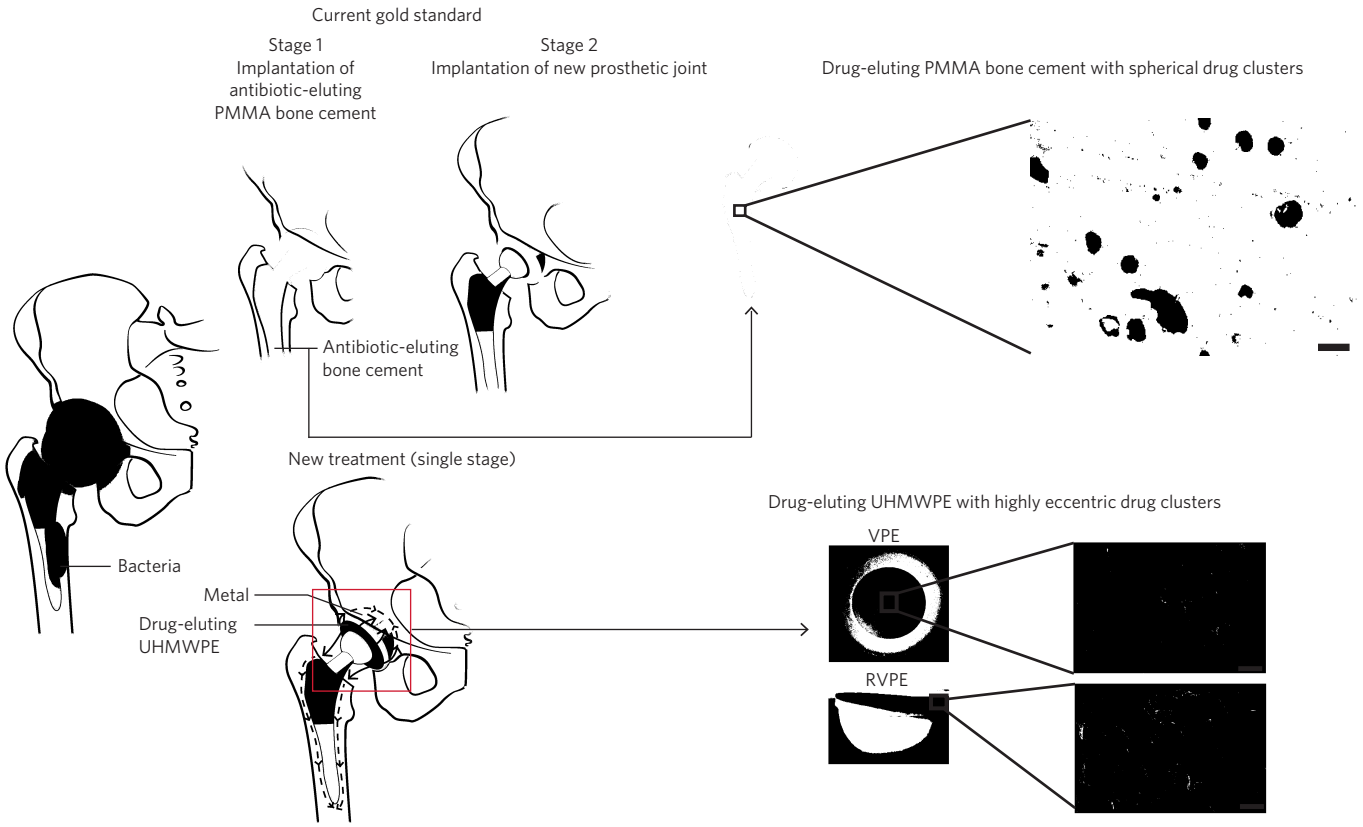

Figure 1 | Highly eccentric drug-eluting polyethylene. The current gold standard of treatment for PJI is two-stage surgery, which involves replacement of the infected prosthesis with antibiotic-eluting PMMA bone cement and intravenous antibiotics (stage 1), then removal of PMMA bone cement and replacement with a new joint prosthesis after bacterial cultures confirm clearance of infection (stage 2). Because of its spherical drug cluster morphology (scanning electron microscopy image, top right), PMMA bone cement requires high drug loading for sufficient drug elution and has weak mechanical strength. Drug-eluting polyethylene with highly eccentric drug clusters allowed much lower drug loading for efficient drug elution, high mechanical strength and a favourable wear rate. Drug-eluting PMMA had spherical drug clusters, which require 30–40% drug content to reach percolation. The high drug loading needed to achieve sufficient drug elution significantly reduces its mechanical strength to the point of insufficient strength for full load bearing. However, drug-eluting UHMWPE with highly eccentric drug clusters (scanning electron microscopy images, bottom right) reached percolation at 6–8 wt% drug content, allowing sufficient drug elution to be reached at a lower content than the antibiotic-eluting bone cement. As a result, the mechanical strength necessary for a fully functional drug-eluting joint prosthesis was maintained and the direct replacement of infected prosthetic joints with new prosthetic joints without immobilization of patients is possible. Scale bars, 100 μm; VPE, 7 wt% vancomycin in UHMWPE; RVPE, 7 wt% vancomycin + 3 wt% rifampin in UHMWPE (red) with underlying non-antibiotic-eluting (unmodified) UHMWPE (white).

was because the percolation threshold was reached at this loading, a much lower concentration than for the conventional spherical cluster system. The elongation at break (Fig. 2b) and the ultimate tensile strength (UTS; Fig. 2c) were highest at a polymer/drug particle size ratio of 4:1.

Highly eccentric drug clusters in UHMWPE

Antibiotic-eluting UHMWPE displaying highly eccentric drug clusters was prepared using compression moulding. Although drug loading at the studied levels increased porosity linearly, the percolation threshold was reached at a drug loading between 4 and 6 wt% (Supplementary Figs 1 and 2), which was corroborated by a sharp increase in drug elution around 6 wt% (Fig. 3a). However, the UTS decreased linearly from 0 to 10 wt% drug loading (Fig. 3b).

We created and utilized an optimization equation to maximize the UTS, impact strength (IS), and drug elution rate (equation (1)). Because UTS, impact strength and elution rate were variable at different scales, their contributions to the optimization were normalized with their respective maximum values (UTS_n, IS_n, and $Rate_n$; UTS and impact strength at 0% drug loading and elution rate by 14% drug loading). In equation (1), C is the drug concentration and t is time.

$$\text{Max}\left(0.5 \times \text{UTS}_\text{n}\left(C\right) + 0.5 \times \text{IS}_\text{n}\left(C\right) + \left(\text{Rate}_\text{n}\left(C, t\right)\right)\right) \quad (1)$$

Solving for this equation showed that the optimum drug loading was 7 wt% (Fig. 3c). Above this concentration, the additional gain in drug elution rate was offset by the decrease in the mechanical properties, while below this concentration the drug elution rate was not sustained at an effective level for treating PJI.

We compared the drug elution of our optimized polymer system with 11 wt% vancomycin in bone cement, which is the highest drug content that can still maintain the industry standard of 70 MPa for compressive strength[28]. The vancomycin elution rate and antibacterial activity of 7 wt% vancomycin-loaded UHMWPE (VPE) was similar to that of 11 wt% vancomycin in bone cement (Fig. 3d and Supplementary Fig. 3), supporting our hypothesis that the highly eccentric drug clusters resulted in more efficient drug release. Vancomycin elution of VPE and bone cement in synovial fluid did not show any statistically significant difference compared with elution in phosphate-buffered saline (PBS) (Supplementary Fig. 4).

The mechanical properties (yield strength, UTS, impact strength and elongation at break) and wear rate of VPE were all within the

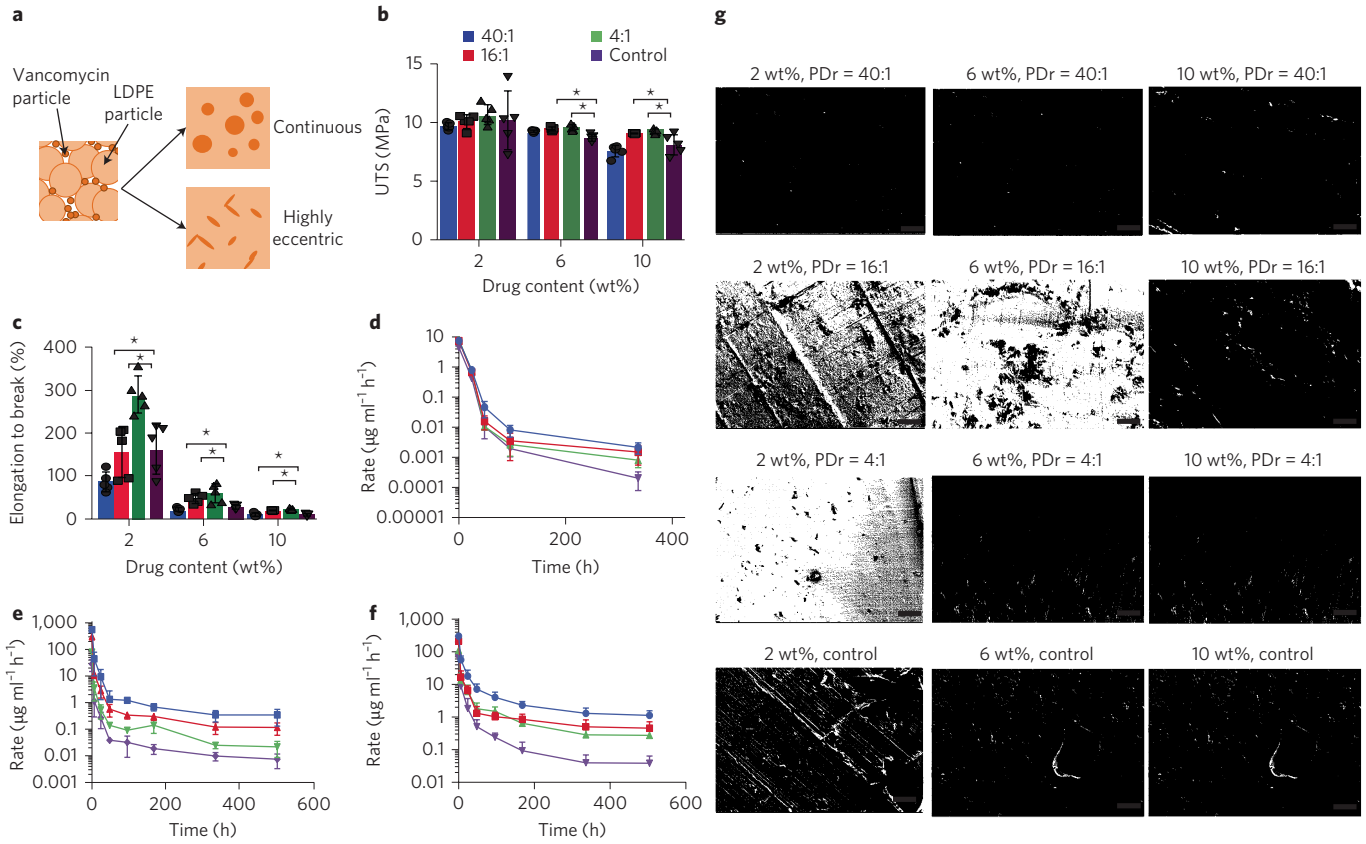

Figure 2 | Highly eccentric drug cluster morphology influences the mechanical and elution properties of the implant material. a, Schematic view of the process for creating highly eccentric drug clusters in LDPE. Vancomycin crystals are interspersed between LDPE particles. Subsequent casting or moulding under minimum flow forms highly eccentric drug clusters. **b**,**c**, UTS (**b**) and elongation to break (**c**) of compression-moulded LDPE (highly eccentric drug clusters) at various LDPE/vancomycin particle size ratios (PDr; 40:1, 16:1 and 4:1) and solvent-cast LDPE (traditional spherical drug clusters, control) at different initial drug loading levels (2, 6 and 10 wt%). **d**–**f**, Vancomycin elution rates from both LDPEs at different drug contents (2 wt% (**d**), 6 wt% (**e**) and 10 wt% (**f**)). **g**, Scanning electron micrograph images of vancomycin-eluting LDPE at various initial drug contents (2 and 10 wt%) under different PDr values (40:1, 16:1 and 4:1) or with vancomycin-eluting LDPE made by solvent casting (control). Scale bars, 100 μm. Drugs were pre-eluted before imaging. For **b**–**f**, data are derived from $n = 5$ per group. Data shown are the means ± s.d.; $^*P < 0.05$.

limit of clinically used UHMWPE[29] (Fig. 3e,f and Supplementary Figs 5–7) and were superior to those of 11% vancomycin-loaded bone cement (Fig. 3e,f).

Drug type and elution rate relationship

We tested nine different antimicrobials (ciprofloxacin hydrochloride (HCl), tobramycin, tetracycline HCl, gentamicin, vancomycin HCl, rifampin, teicoplanin, ceftriaxone and fusidic acid) that spanned different polar surface areas (PSA; 72–663 Å^2) and molecular volumes (MV; 282–1600 Å^3) (ref. [30]). The ratios of these values (PSA/MV) were used to normalize polarity by molecular size. In UHMWPE with highly eccentric drug clusters (Supplementary Fig. 8), more polar compounds (PSA/MV > 0.3) had higher early elution rates, but these dropped more rapidly over time, compared with non-polar compounds (PSA/MV < 0.3) (Supplementary Fig. 9). Therefore, drugs with a large polar surface area or small molecular volume (low PSA/MV) can be advantageous in applications that require a potent, short-term release of medication, such as local anaesthetics (bupivacaine, lidocaine, ropivacaine) and antifibrinolytics (tranexamic acid). However, drugs with a smaller polar surface area or larger molecular volume (high PSA/MV) can be advantageous in applications that require a less potent initial release, but sustained elution. For example, pertinent to PJI treatment, rifampin is an antimicrobial that is highly effective at the time-dependent eradication of *Staphylococcus aureus* biofilm[31], but is also hepatotoxic at high concentrations. Therefore, sustained and lower concentration drug release can be beneficial for bacterial eradication, while minimizing the side effects.

Irradiated VPE enhances antibacterial properties

Most clinically used prosthetic joints are irradiated either for sterilization (25–40 kilogray (kGy); ref. [32]) or for cross-linking (>50 kGy; ref. [33]). Sterilization dose (~25 kGy) did not affect the UTS, impact strength, elution profile or wear rate (Supplementary Fig. 6), compared with those of unirradiated VPE. High dose irradiation (100 kGy) decreased the UTS, impact strength and wear rate (5.4 mg per million cycles (mg MC^{-1})), but did not affect the elution rate (Supplementary Fig. 10).

After vancomycin was eluted for six months and no further elution of vancomycin could be detected by liquid chromatography (detection limit = 0.1 μg ml^{-1}), 25- and 100-kGy irradiated VPEs showed less bacterial adherence than unirradiated VPE (Fig. 3g). Immunofluorescence staining of vancomycin showed fluorescence on the surfaces of the irradiated VPEs, but not on unirradiated VPE (Fig. 3h and Supplementary Fig. 11), indicating the presence of vancomycin on the surfaces of the VPE after all elutable drug was released. This suggested that some vancomycin was immobilized in the UHMWPE as a result of irradiation, presumably by grafting through its phenolic hydroxyl group[34].

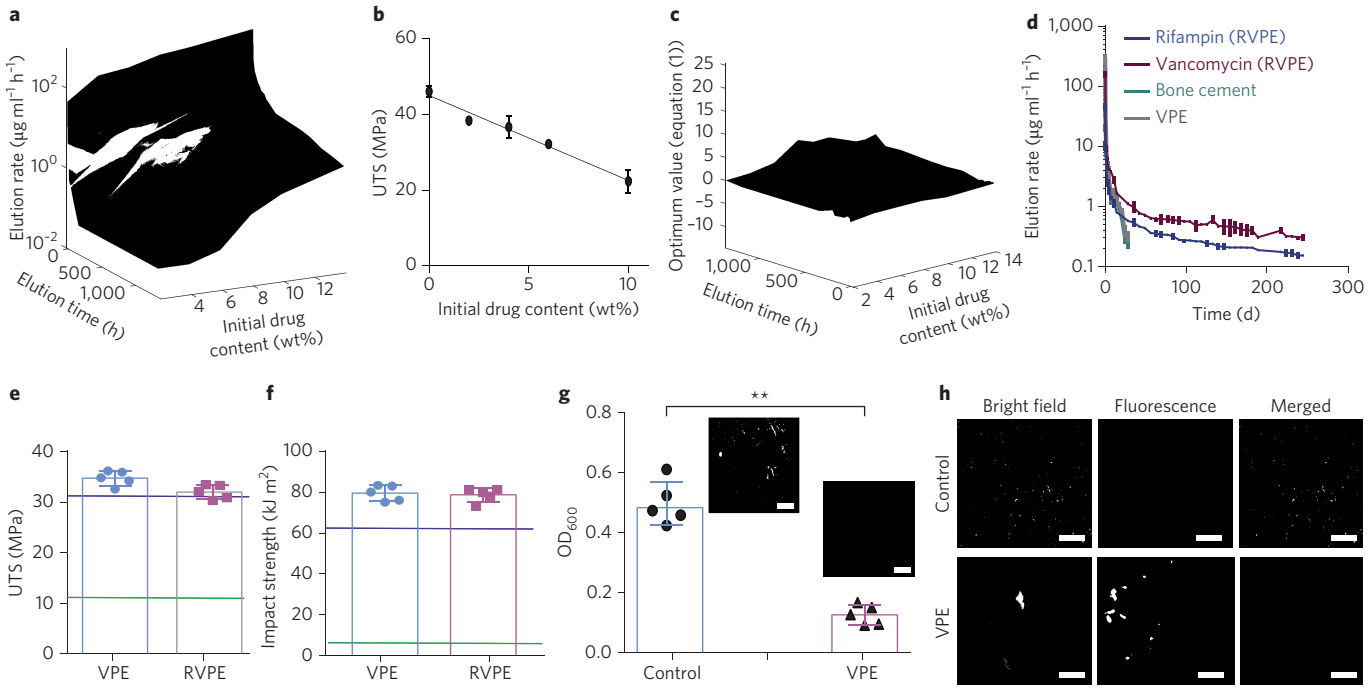

Figure 3 | Influence of the highly eccentric morphology of modified UHMWPE on its drug elution and mechanical properties. a, Response surface of vancomycin elution rate, elution time and initial vancomycin content of highly eccentric morphology in vancomycin-eluting UHMWPE. **b**, Relationship between UTS and initial drug content ($n = 5$). **c**, Response surface optimization of equation (1) for drug content in UHMWPE and elution time. **d**, Elution rate of rifampin and vancomycin from RVPE and that of vancomycin from VPE and bone cement (11 wt% vancomycin loading, bone cement) ($n = 5$). **e**,**f**, UTS (**e**) and impact strength (**f**) of VPE and RVPE. Green line indicates the mean value of bone cement. Purple line indicates the minimum value of clinically used UHMWPE[29] ($n = 3$). **g**, UHMWPE with no antibiotics (control) and VPE were pre-eluted for six months, then incubated with *S. aureus* for 24 h. Adherent bacteria were quantified by sonication and subsequent incubation for 24 h ($n = 5$); **, $P < 0.01$. Inset: fluorescently labelled adherent live (green) and dead (red) bacteria. **h**, Fluorescence labelling of surface-bound vancomycin with mouse anti-vancomycin and fluorescently labelled goat anti-mouse. Samples were pre-eluted for six months before labelling. Scale bars, 100 μm; data shown are the means ± s.d.

VPE eradicates planktonic *S. aureus*

An intra-articular PJI model was created by implanting osteochondral plugs of VPE, non-antibiotic containing UHMWPE and a commonly used bone cement spacer formulation[35] (containing 8.3 wt% tobramycin sulfate and 2.3 wt% vancomycin HCl; VTBC) in the femoral trochlear groove, and a titanium plug with a porous surface in the tibial plateau of skeletally mature New Zealand white rabbits. All rabbits received two bacterial suspensions (5×10^7 CFU ml^{-1} each) that were injected in the distal tibial canal and the intra-articular space (Fig. 4a,b). None of the rabbits received any antibiotics for the duration of the study (3 weeks).

Overall, 60% of VPE and 40% of VTBC rabbits survived compared with none of the rabbits that received UHMWPE plugs without any antibiotics (Fig. 4e). Immediately post-surgery, no difference in gait and joint movement was observed between control, VTBC and VPE groups. However, after several days, the infected knees of the control rabbits were more swollen, retracted and passive, than the VTBC and VPE rabbits. No mechanical failure including deformation, fracture, delamination or pitting was observed in the retrieved implants. Bioluminescence imaging of the knee joints at the endpoint, two-photon live/dead imaging and sonication and culturing of joint tissues and implants (Fig. 4c–h and Supplementary Figs 12 and 13) did not show any bacterial growth on any component for the rabbits implanted with VPE, suggesting the complete eradication of bacteria. However, significant amounts of live bacteria were found on all rabbits receiving VTBC, albeit in lesser amounts than the control, indicating ongoing infection in the VTBC group.

Since vancomycin can be toxic[36], the serum vancomycin concentration was determined. No vancomycin was detected systemically in any of the rabbits at any time point (detection limit 10 ng ml^{-1}). Kidney function byproducts (creatinine and body urea nitrogen) and liver function enzymes (alanine aminotransferase and alkaline phosphatase) remained within normal limits for all rabbits in the VPE group for the duration of the study (Supplementary Fig. 14). These results confirmed the efficacy of vancomycin eluted from radiation sterilized VPE *in vivo*.

Drug-eluting UHMWPE against biofilm

In PJI, the bacterial biofilm is often localized at the bone–implant interface, which is difficult to eradicate due to limited antibiotic penetration administered systemically[37]. The combination of rifampin and vancomycin is the state-of-the-art treatment used against bacterial biofilm[38], and can synergistically act against both Gram-positive and Gram-negative bacteria[39]. The synergy reduces the MIC for vancomycin and can hinder the rapid bacterial resistance associated with rifampin alone[40], by tailoring the concentration ratios of vancomycin to rifampin such that the concentration of vancomycin is higher for the duration of the release.

Based on clinical guidelines for vancomycin/rifampin concentration ratios for the treatment of PJI (Supplementary Table 1), incorporation of a 2.5:1 vancomycin/rifampin ratio allowed long-term maintenance of a vancomycin/rifampin elution rate ratio closest to the clinically desired trough ratio (Supplementary Fig. 15). The vancomycin elution rate was consistently higher than the rifampin elution rate for UHMWPE incorporated with 3 wt% rifampin in addition to 7 wt% vancomycin (RVPE; Fig. 3d) and the vancomycin elution rate from RVPE was significantly higher than that from VPE and bone cement (Fig. 3d). Rifampin and vancomycin elution of VPE and bone cement in synovial fluid was not significantly different than elution in PBS (Supplementary Fig. 4). Pre-eluting

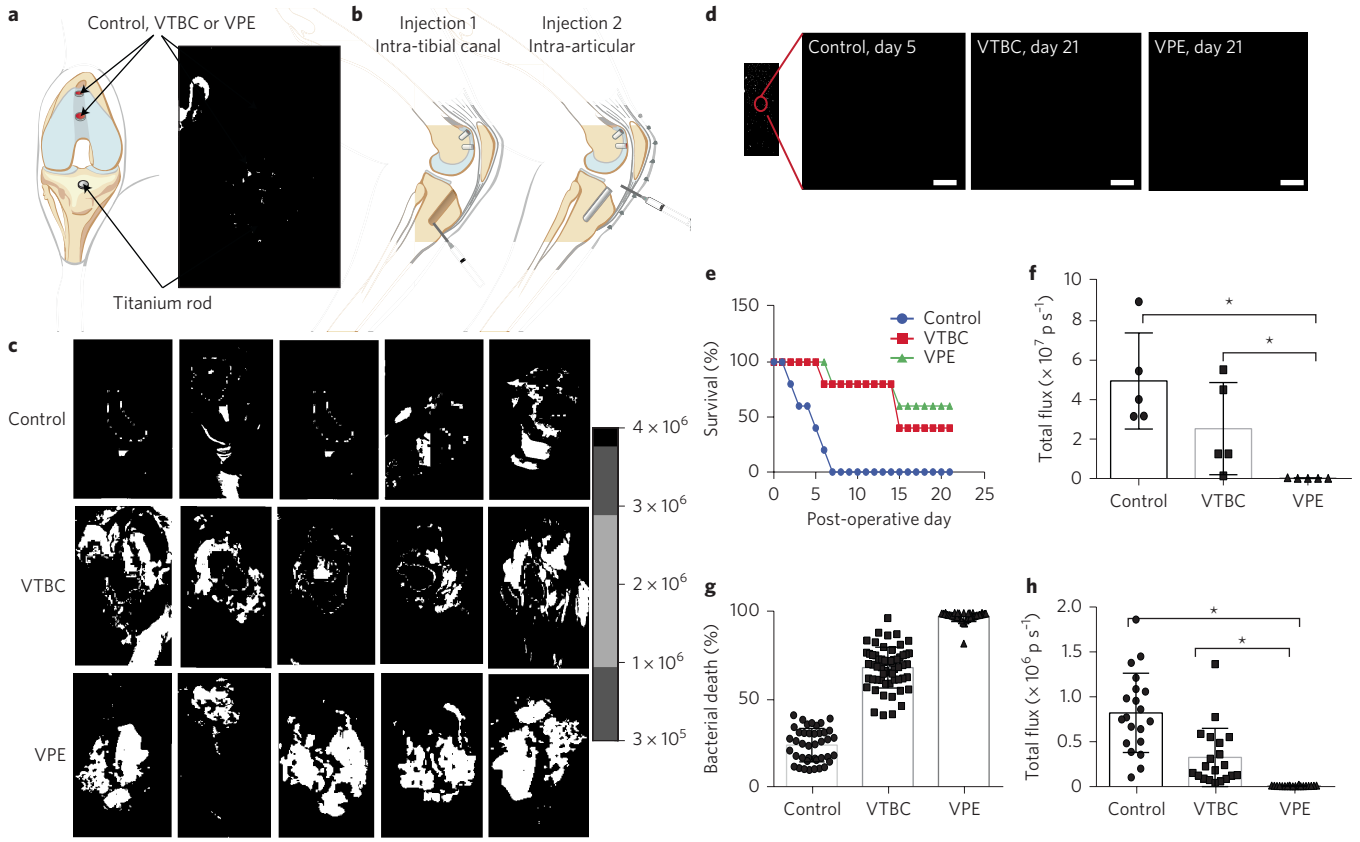

Figure 4 | *In vivo* evaluation of VPE in joint infection model. a, Schematic and representative gross view of implantation of non-antibiotic-eluting-PE (control), VTBC, VPE and titanium rod. **b**, Schematic of bacterial injection sites for the two bacterial injections administered to all rabbits. **c**, Bioluminescent imaging of rabbit knee joint with implanted control, VTBC, VPE and titanium rod. Bioluminescent imaging was conducted immediately after each animal either died or was euthanized at the experimental endpoint. **d**, Representative two-photon live/dead imaging of adherent live (green) and dead (red) bacteria on the explanted titanium. Scale bars, 200 μm. **e**, Survival of the rabbits in the control, VTBC and VPE groups. All controls died within one week, while 40% of VTBC and 60% of VPE rabbits stayed alive until the end of study ($n = 5$ per group, $P < 0.01$ log-rank test). **f**, Total average bioluminescence of the rabbit knees shown in **c**. **g**, Mean percentage bacterial death of the bacteria adherent to the surface of the titanium rods post-explant. **h**, Mean bioluminescence post-sonication and after 12 h reculturing; calculated by averaging total flux for the femur, tibia, implants, patellar tendon and quadriceps tendon from all rabbits in the same group. Data shown are the means ± s.d., $^*P < 0.05$.

the RVPE for one year and then exposing it to a liquid culture of *S. aureus* still prevented the bacteria from growing, indicating that the antibiotics eluted from RVPE were still above the MIC for this microorganism in biofilm form. Mechanical strength (UTS and impact strength) and wear rate were within the limit of clinically used UHMWPE (Fig. 3f and Supplementary Figs 5–7).

RVPE with a total drug concentration of 10 wt% was localized only in the surface, unloaded regions[17,18], to minimize the effect of the increased drug concentration on the mechanical properties of the potential implant (Fig. 1). Our previous work in spatially controlling the morphological properties of UHMWPE, by layering different compositions of UHMWPE during compression moulding, showed integrity at the interface[41].

An *in vitro* simulation of biofilm formation at the bone–implant interface of a joint implant was done by sandwiching bone, titanium and UHMWPE (Fig. 5a). A bioluminescent *S. aureus* (Xen 29, PerkinElmer) biofilm was grown on the porous surface of titanium discs for 48 h. The surfaces were clamped together, with the biofilm-laden porous titanium surface in contact with the bone and the non-porous surface in contact with UHMWPE (Fig. 5b). The average synovial fluid volume and the size of the femoral component of a knee implant were used to scale down the size of the RVPE, the volume of media and the bone–titanium interface, respectively (Supplementary Table 2). The average biofilm thickness was 25.5 ± 2.2 μm, in agreement with previous reports[42]. The biofilm was completely eradicated in the sandwiches with RVPE by 48 h (Fig. 5c). Two-photon live/dead fluorescence excitation imaging of the titanium beads revealed >95% biofilm eradication in the RVPE group within 96 h, while the bacteria viability in the controls remained consistently elevated for 2 weeks (Fig. 5d,e). These results suggested that the antibiotics eluted from the UHMWPE implant surfaces could reach therapeutic levels at the bone–implant interface.

In an adaptation of the PJI model for acute infections with planktonic bacteria above, all rabbits received a titanium rod with fully grown bioluminescent *S. aureus* biofilms in the tibial canal (Fig. 6a). There was no statistically significant difference in bioluminescence between the three groups (control, VTBC and RVPE) before implantation (Fig. 6b). None of the rabbits received any systemic antibiotics for the duration of the study (3 weeks). All control rabbits and 80% of rabbits receiving VTBC expired, whereas all rabbits in the RVPE group survived for 3 weeks (Fig. 6f). Because live bacteria were found in the joints during the postmortem analysis (Fig. 6c,d), we suspect that some of the bacteria spread hematogenously and caused sepsis. Immediately post-surgery, no difference in gait and joint movement was observed between control and RVPE groups. However, after several days, the infected knees in the control and VTBC rabbits were more swollen, retracted and passive than those in the RVPE rabbits. No mechanical failure, including deformation, fracture, delamination or pitting was observed in the retrieved implants. No live bacteria were observed in the RVPE

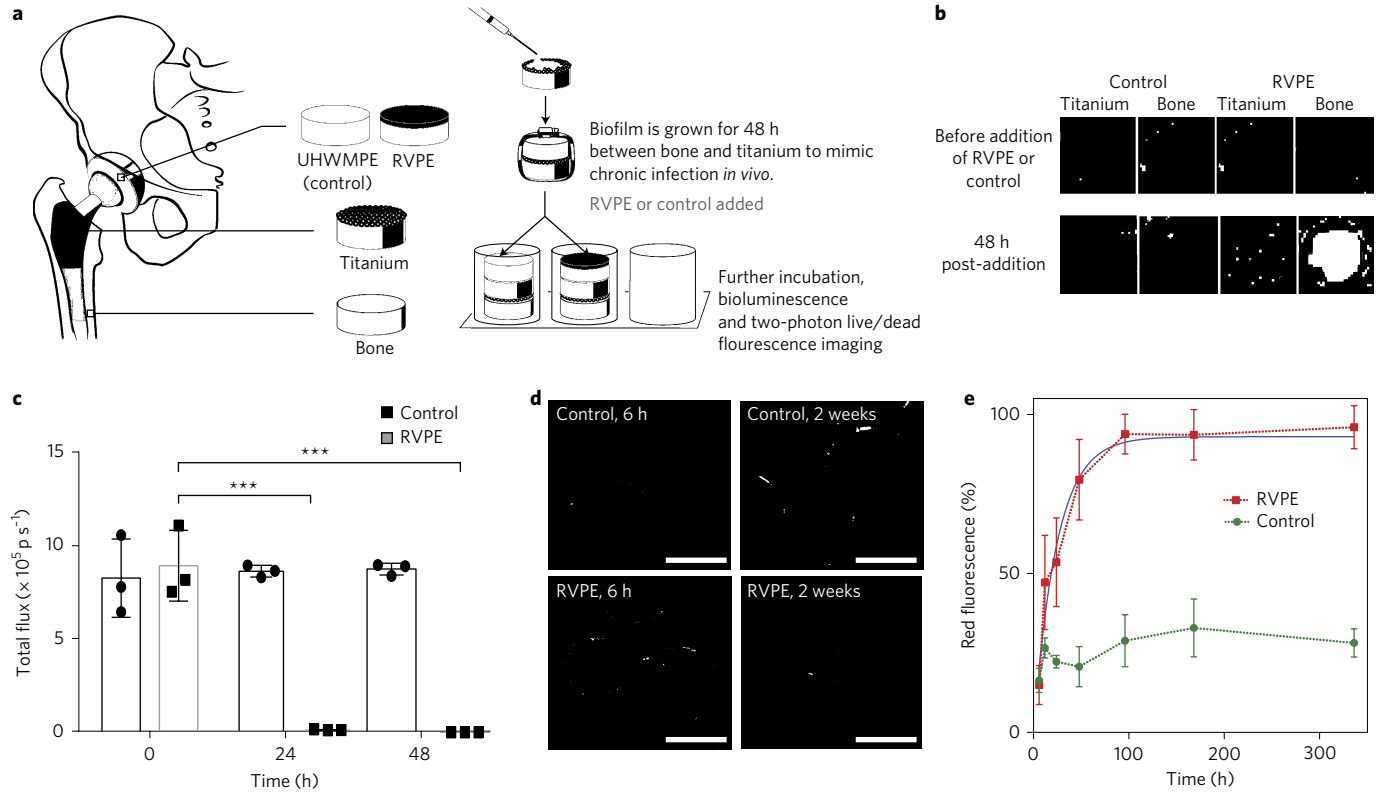

Figure 5 | *In vitro* evaluation of RVPE. a, Schematic of 'sandwich' experiment to treat bacterial biofilm between bone and titanium using either non-antibiotic-eluting UHMWPE (control) or RVPE. Bacterial biofilm is often found between titanium and bone surfaces in patients with chronic PJI. Bioluminescence was measured for all 21 constructs. At predefined time points (6 h, 24 h, 48 h, 96 h, 120 h, 1 week and 2 weeks; $n = 3$ each for each time point), bone and titanium were live/dead stained and imaged with two-photon fluorescence microscopy. **b**,**c**, Bioluminescent imaging (**b**) and its quantification (**c**) at the titanium–bone interface after 24 h and 48 h with RVPE or control treatment ($n = 3$, $^{***}P < 0.001$). **d**, Two-photon live/dead imaging of the bacteria that adhered to the surface of titanium at 6 h and 2 weeks after treatment with the control or RVPE. Scale bars, 200 μm. **e**, Percent live/dead as a function of time of exposure in the control and RVPE treatments. Data are means ± s.d.

group, according to bioluminescence (Fig. 6c and Supplementary Fig. 16), two-photon live/dead imaging (Fig. 6e,g), and sonication with subsequent culturing of joint tissues and implants (Supplementary Fig. 17). Kidney function byproducts (creatinine and body urea nitrogen) and liver function enzymes (alanine aminotransferase and alkaline phosphatase) remained within normal limits for all rabbits in the RVPE group during the study (Supplementary Fig. 18). These results confirmed the efficacy of this potential implant material against a *S. aureus* biofilm *in vivo*.

Because of the potential inhibition of implant fixation due to high dose rifampin[43], we tested the effect of RVPE implants on the bony ongrowth to the surface of metal screws (see Methods). To create the most clinically relevant model, the ratio of the RVPE surface area to the bone–implant interface in the murine model was matched to those observed in the human knee (Supplementary Table 3). RVPE ($n = 4$) or control UHMWPE ($n = 4$) plugs were implanted in the distal femur, while a stainless steel screw was implanted on the femur (Supplementary Fig. 19a). All rats were euthanized six weeks post implantation. Bony ongrowth to the metal was observed in all rats (Supplementary Fig. 19b). No statistically significant difference in bone volume/total volume ratio (BV/TV) of bone surrounding the screws was observed (Supplementary Fig. 19c).

Discussion

We report a new method of making a drug-eluting polymer with highly eccentric drug clusters. This results in improved mechanical strength and sustained drug elution at lower drug loading, compared with conventional polymers with spherical drug clusters (Fig. 1). The method was applied to both low- and high-melt flow index polymers (for example, UHMWPE and LDPE, respectively). There is the possibility of applying this technique to other commonly used drug-eluting polymer systems, such as poly(lactic-*co*-glycolic acid). In addition, the effects of drug chemistry and structure have been studied, while maintaining the highly eccentric morphology (Supplementary Fig. 4), to evaluate the possibility of using this morphology for other drug–polymer combinations to treat various diseases. Due to higher interconnectivity, the highly eccentric drug clusters in polyethylene enabled the reduction of the drug percolation threshold from very high drug loading (40–60 wt%) (ref. [23]) to 6–8 wt% (Supplementary Figs 1 and 2 and Fig. 3a). The interconnected morphology also resulted in drug elution that was sustained for a longer duration (Fig. 2d–f) and had a higher mechanical strength (Fig. 2b,c), compared with drug-eluting polyethylene with spherical drug clusters. Lower initial drug loading may also imply a higher safety margin in adverse scenarios, where incorporated drugs may be unintentionally released.

Polymeric matrices can be effective local delivery devices because they enable more effective drug delivery than through systemic administration; they can also enhance the efficacy of the incorporated drugs by targeting the required location of treatment[44]. Common strategies involve injectable, drug-eluting polymers in the form of microspheres[45] or micelles[46], but degradation products can be toxic[47], drug elution rates can fall below effective levels[46], and drug release can have low efficacy[46]. The gold standard for drug-incorporated polymers in treating PJI is antibiotic-eluting bone cement made of polymethylmethacrylate (PMMA)[13], which

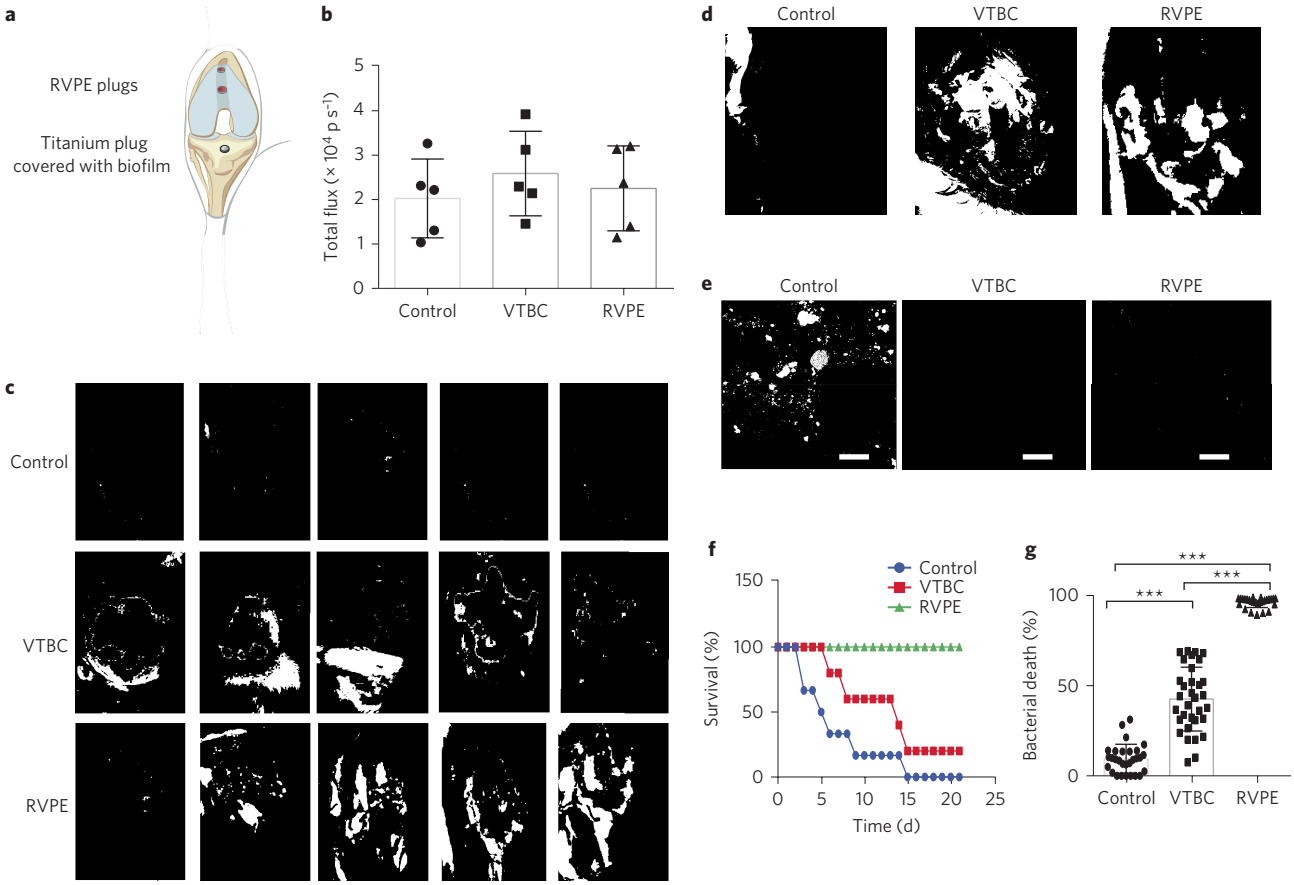

Figure 6 | *In vivo* evaluation of RVPE in a lapine joint infection model. a, Schematic view of implantation of non-antibiotic-eluting UHMWPE (control), VTBC, RVPE and titanium rod in lapine intra-articular model. **b**, Mean bioluminescence of the titanium rods before implantation in rabbits. **c**, Postmortem bioluminescent imaging of rabbit knee joints from VTBC and RVPE groups. All rabbits were alive at day 21 in the RVPE treatment. **d**, Representative gross image of a dissected knee from the control, VTBC and RVPE groups. Copious amounts of pus were found in the knee joints of the control and VTBC rabbits, whereas no pus was found in the knee joints of the rabbits treated with RVPE. **e**, Representative two-photon live/dead imaging of the live (green) and dead (red) bacteria on the titanium rods after retrieval. Scale bars, 200 μm. **f**, Survival of the rabbits during the experimental period; none of the control, 20% of VTBC and 100% of RVPE rabbits survived to the end of study; $P < 0.01$, comparing the control versus RVPE and VTBC versus RVPE groups by log-rank test. **g**, Mean percent bacterial death of the bacteria that were adhered to the surface of the titanium rods after retrieval. Data are means ± s.d; $^{***}P < 0.001$.

can only be used in limited load-bearing applications[48]. A fully load-bearing permanent implant using UHMWPE can address the shortcomings of other drug-eluting polymers in joint replacement. The reported highly eccentric drug clusters combined with our spatially controlled consolidation technology can enable the sustained delivery of state-of-the-art antibiotic combinations, without sacrificing the required mechanical properties of the implant. The long track record of safety and efficacy of UHMWPEs[33], combined with well-known antibiotics such as vancomycin and rifampin, has the potential of eliminating the use of antibiotic-eluting spacers and reducing the gold standard two-stage treatment surgeries for PJI to a single surgery. Based on the effects of increasing antibiotic concentration on the mechanical properties of UHMWPE and the contact stresses of the joint[49], we proposed several implant designs (Supplementary Table 4). All of the designs provided have mechanical strengths and wear rates within the range of clinically used UHMWPE (conventional UHMWPE and highly cross-linked UHMWPE (HXLPE); Supplementary Table 3). The uniform vancomycin-containing UHMWPE (7 wt%; VPE) and VPE with a surface layer of rifampin and vancomycin-containing UHMWPE (10 wt%) are intended for temporary (6–8 weeks) usage or for longer term usage in patients with low activity, because the wear rates were closer to conventional UHMWPE than HXLPE. Virgin UHMWPE with a surface layer of rifampin and vancomycin-containing UHMWPE (10 wt%; RVPE) can be used for long-term applications (years), because its articulating surface is composed of HXLPE with the lowest wear rate.

In addition to the risk of mechanical failure during weight bearing, antibiotic-eluting PMMA bone cements showed bacterial adhesion[50] even during antimicrobial elution[51]. However, radiation sterilized VPE significantly reduced bacterial adherence through surface-bonded vancomycin (Fig. 3g,h). This is in agreement with previous reports on vancomycin grafting on titanium, which prevented biofilm formation on its surface[52]. Reduction of bacterial adherence reduced the infection rate[53]. Surface-bound vancomycin eradicated bacteria by making the peptidoglycan layer that is essential to biofilm formation less rigid and more permeable. As a result, the osmotic pressure can cause bacterial death[52]. In addition to sustaining effective concentrations of antibiotic elution for bacterial eradication, grafting of the antibiotic by irradiation may further hinder bacterial attachment in antibiotic-eluting UHMWPE in the longer term.

VPE and RVPE outperformed clinically used antibiotic-eluting bone cement VTBC in planktonic and biofilm PJI models, respectively. The ability of VTBC to control the bacterial concentration was better in the planktonic model than in the biofilm model, presumably because bacterial susceptibility to vancomycin and tobramycin decreased by at least 1,000-fold in biofilm form[54]. While

similar survival rates were observed for animals treated with VPE and VTBC, VPE (but not VTBC) completely eradicated all the bacteria in the joint. This may be partly due to the higher susceptibility of Xen29 to vancomycin[55] than to tobramycin[56].

Usage of antibiotics intravenously, orally, in the form of antibiotic-eluting bone cement, VPE and RVPE, all come with a risk of developing resistant bacteria. Even when bacteria were exposed to 200 times their MIC, they could develop resistance within 10 h (ref. [57]). This suggests that our previous understanding that bacterial resistance is directly related to being exposed to below-MIC concentrations of antibiotics[58] may be incomplete. Nevertheless, by matching the vancomycin elution of VPE to clinically used vancomycin-eluting bone cement (Fig. 3d), we expect VPE to pose no extra risk in bacterial resistance development to antibiotic-eluting bone cement. In the case of RVPE, by creating elution of vancomycin that exceeds the antibiotic-eluting bone cement (Fig. 3d) and by ensuring that vancomycin elution is always higher than that of rifampin to prevent sole exposure of bacteria to rifampin, we also expect that RVPE will not pose any extra risk of bacterial resistance development to antibiotic-eluting bone cement.

Loading UHMWPE with therapeutic agents using highly eccentric drug clusters could potentially address problems, such as pain, osteolysis, osteoporosis and infection, in joint arthroplasty and other orthopaedic fields, such as trauma and spine. In addition, the application of this morphology to other drug–polymer matrices could benefit treatment in other applications where both drug elution and mechanical strength are crucial for the success of implants.

Methods

General experimental approaches. No samples, rabbit or data points were excluded from the analyses. Samples were not randomized to experimental groups unless specified. Lapine experiments and analyses were not performed in a blinded fashion.

Solvent casting of vancomycin-eluting LDPE with spherical drug clusters. LDPE was dissolved slowly in boiling xylene (138 °C) to reach a concentration of 60 mg ml^{-1}. After all the LDPE had dissolved, the resulting solution was then cooled to 110 °C. Under mechanical stirring, vancomycin crystals, size <75 µm, were added to reach the desired weight percent with respect to the LDPE content (0–10 wt%) and kept at 110 °C for 30 minutes to further remove the solvent. The resulting viscous solution was transferred to a stainless steel rectangular mould (50 mm × 85 mm) and put in a vacuum oven, with a vacuum pressure of −0.1 MPa, at 90 °C to further remove the solvents.

Manufacture of vancomycin-eluting LDPE with highly eccentric drug clusters. LDPE pellets were cryomilled and then sieved to the appropriate desired particle size range. Vancomycin HCl was crushed with a mortar and pestle and then passed through a 75 µm sieve. To create vancomycin-eluting LDPE with 7 wt% drug loading, 0.7 g of the sieved vancomycin powder was mechanically mixed with 9.3 g of the cryomilled LDPE powder for 30 min at room temperature. The resulting mixture was transferred to a rectangular mould (50 mm × 85 mm) and compressed at 25 °C for 1 min at 10 MPa. The compressed solid mixture was subsequently heated at −0.1 MPa and 190 °C for 30 min and then compression moulded at 10 MPa for 1 min before being cooled to 25 °C at a rate of 10 °C min^{-1}.

Manufacture of optimized vancomycin-eluting UHMWPE with highly eccentric drug clusters (VPE). Vancomycin HCl (1.75 g) was crushed with a mortar and pestle and then passed through a 75 µm sieve. The vancomycin powder was mechanically mixed with GUR1020 UHMWPE powder (Celanese, 23.25 g) for 30 min at room temperature to obtain a 7 wt% vancomycin-blended UHMWPE and poured into a circular mould (10.5 cm inner diameter). The vancomycin-UHMWPE mixture was then consolidated by compression moulding at 170 °C and 20 MPa, for 5 min. The resulting consolidated VPE was cooled, at a rate of 10 °C min^{-1}, to room temperature to yield approximately 3-mm-thick and 10.5-cm-diameter vancomycin-blended UHMWPE.

Manufacture of optimized rifampin-vancomycin-eluting UHMWPE with highly eccentric drug clusters (RVPE). Rifampin (0.4 g) was crushed with a mortar and pestle and passed through a 75 µm sieve. Vancomycin HCl (0.8 g) was crushed with a mortar and pestle and passed through a 75 µm sieve. The rifampin and vancomycin HCl powders were then mechanically mixed for 30 min at room temperature. GUR1020 UHMWPE (12 g) was added to the rifampin and vancomycin HCl mixture, which was then mechanically mixed/blended for 30 min at room temperature, to obtain a 3 wt% rifampin and 7 wt% vancomycin-blended UHMWPE. The resulting rifampin and vancomycin-blended UHMWPE (10 g) was transferred and spread evenly onto a circular stainless steel mould (11 cm inner diameter). GUR1020 UHMWPE without additives (25 g) was then added and spread evenly on top of the rifampin and vancomycin-blended UHMWPE. The resulting constructs were consolidated by compression moulding at 170 °C and 20 MPa, for 5 min, before being cooled at a rate of 10 °C min^{-1} to room temperature.

Manufacture of vancomycin-eluting PMMA bone cement. Vancomycin HCl (5 g) powder that had been crushed with a mortar and pestle and passed through a 75 µm sieve was mechanically mixed with PMMA powder (27 g; Simplex P, Stryker) for 30 min at room temperature. After thorough mixing, the cement's liquid monomer (13.5 g) was added and then mixed thoroughly with a spatula. The vancomycin-cement dough was poured into a stainless steel mould to form its final shape. After about 15 min, the hardened vancomycin-eluting PMMA bone cement was removed from the mould.

Manufacture of clinically relevant PMMA bone cement spacer (VTBC). Tobramycin sulfate (3.6 g) and vancomycin HCl powder (1 g) that had been crushed with a mortar and pestle and passed through a 75 µm sieve was mechanically mixed with PMMA powder (30 g) for 30 min at room temperature. After thorough mixing, the cement's liquid monomer was added and then mixed thoroughly with spatula. The antibiotic-containing cement dough was poured into a stainless steel mould to form its final shape. After about 15 min, the hardened VTBC was removed from the mould. VTBC samples were ethylene oxide sterilized before implantation.

***In vitro* drug release from drug-eluting UHMWPE and drug-eluting PMMA bone cement.** For drug-eluting UHMWPE, blocks (5 mm × 5 mm × 20 mm; $n = 6$) were cut from the consolidated samples. For drug-eluting PMMA bone cement, vancomycin-cement dough was poured into a stainless steel mould to form 5 mm × 5 mm × 20 mm blocks. Each block was immersed in 1 ml PBS at 37 °C; after 6 h, 24 h, every 24 h for 1 week, and then once every week up to 12 months, the blocks were washed with PBS and placed in new PBS (1 ml). Concentrations of vancomycin and rifampin were determined using ultraviolet–visible spectroscopy (UV–vis; Cary100, Varian) at 280 nm (vancomycin) and 450 nm (rifampin). The rate of drug release was calculated by dividing the measured concentration by the duration that the sample had been in contact with PBS.

Scanning electron microscopy. All LDPE, UHMWPE and PMMA bone cement samples were sputter coated with a thin layer of gold/palladium and imaged on a Zeiss Supra55VP microscope. Both Everhart–Thronley and Inlens detectors were used to acquire the image.

Structural analysis of drug-eluting UHMWPE with highly eccentric drug clusters using micro-computed tomography (micro-CT). Tomograms of cylindrical pins (9 mm diameter, 5 mm long) were acquired and three-dimensional (3D) reconstruction was perfomed using a cone-beam X-ray scanner (µCT 40, Scanco Medical) with a voxel resolution of ~10 µm. Porosity analysis and pore accessibility were analysed using the iMorph software package (version 3.1; www.imorph.fr)[59]. The resulting tomogram was then thresholded to partition between the pores and the polymeric matrix. Porosity was calculated by dividing the volume belonging to the pore to the total volume of the samples. The accessible porosity module implanted in iMorph allowed quantification of the pore volume accessible from one side of the sample by a particle depending on its size.

Tensile strength measurement. Type V samples ($n = 5$ for each group) were stamped out of 3.2-mm-thin sections of the materials mentioned above according to ASTM-D638. These samples were tested in tension (Insight) with a crosshead speed of 10 mm min^{-1}. The stress and strain were recorded at 100 Hz and the gauge length was monitored using a laser extensometer. The engineering stress–strain curves were calculated using the crosshead displacement. The UTS, yield strength, elongation at break, work to failure, and Young's modulus (E) were calculated.

Fracture toughness measurement. Samples (63.5 mm^3 × 12.7 mm^3 × 6.35 mm^3; $n = 5$) were double notched according to ASTM-D256 and were impact fractured with a hammer (CEAST Instron). The energy loss of the pendulum after impact was recorded as the impact strength of the samples.

Determination of wear rate by bidirectional pin-on-disc test. Cylindrical pins (9 mm diameter, 13 mm long; $n = 3$ for each group) were machined using a computer numerical control (CNC) mill (ShopBot) from the materials prepared above. The pins were wear tested with a rectangular pattern (5 mm × 10 mm) against polished cobalt–chromium (CoCr) discs at 2 Hz in undiluted, preserved bovine serum as a lubricant. The pins were cleaned and weighed before testing and at every 0.16 MC after the first 0.5 MC up to 1.2 MC. The wear rate was determined by a linear regression of the weight loss as a function of the number of cycles from 0.5 to 1.2 MC.

Antibacterial activity of VPE and vancomycin-eluting PMMA bone cement. Relative antibacterial activity of VPE and bone cement was assayed using a protocol modified from ref. [60]. Cylindrical discs (8 mm diameter, 3 mm thick) of VPE and vancomycin-eluting PMMA bone cement were sterilized using ethylene oxide. Test organisms (*S. aureus*, ATCC 29213 and *Staphylococcus epidermidis*, ATCC 35984) were cultured in tryptic soy broth at 37 °C for 24 h and subsequently plated to Mueller–Hinton II agar at 37 °C for 18 h. Three to five colonies were then selected and suspended in Mueller–Hinton II broth and the inoculum concentration was adjusted to 0.5 McFarland turbidity standards. The surface of a new Mueller–Hinton II agar plate was then covered uniformly with bacterial suspension using a sterile swab. Samples were placed on the surface of the Mueller–Hinton II agar plates that had been seeded with either the *S. aureus* or *S. epidermidis* strains and further incubated at 37 °C for 24 h. Pictures of the back of the plates and a ruler were taken. The area of inhibition (that is, the clear area with no sign of bacterial growth) was measured using Image J software (version 1.5). When bacteria grew to the immediate surroundings of the implants, the inhibitory area was $3.14\times4\times4=50.24\,mm^2$. Samples were transferred to new Mueller–Hinton II agar plates that had been seeded with either *S. aureus* or *S. epidermidis*. These steps were repeated every 24 h for 3 weeks.

Determination of vancomycin grafting on gamma-beam-irradiated UHMWPE. VPE, RVPE and UHMWPE with no antibiotics (the control) were incubated in PBS for 12 months; the PBS was replaced every week until the end of the study. At 12 months, no vancomycin and rifampin was detected by either UV–vis or high-performance liquid chromatography (HPLC; Agilent 1200 series) and mass spectroscopy (MS; Agilent 6310 Ion Trap mass spectrometer). Samples were washed twice with PBS and blocked for 30 min using 10% fetal bovine serum in distilled, deionized water (blocking buffer). Samples were then incubated with mouse anti-vancomycin immunoglobulin-M (IgM) (1:300; U.S. Biologicals) in blocking buffer at 4 °C for 12 h, washed with PBS and incubated with AlexaFluor 488-coupled goat anti-mouse IgM (A-21042, Thermo Fisher) diluted 1:300 in blocking buffer at room temperature for 1 h. Samples were washed three times in PBS, followed by two 30 min incubations in PBS. Particles were visualized using an inverted fluorescence microscope (Nikon Eclipse TE2000).

Antibacterial activity of surface-bonded vancomycin on gamma-irradiated UHMWPE. VPE, RVPE and UHMWPE with no antibiotics (the control) were incubated in PBS for 12 months; the PBS was replaced every week until the end of the study. At 12 months, no vancomycin and rifampin was detected by either UV–vis or HPLC. Samples were washed in PBS and sterilized with ethylene oxide before incubation in 1 ml of 1% dextrose/PBS. *S. aureus* was cultured in trypticase soy broth for 12 h. The culture was pelleted by centrifugation at 3,200 ×*g* for 5 min and then resuspended in Mueller–Hinton II broth to create $1.5\times10^8\,cfu\,ml^{-1}$ using 0.5 McFarland standard. The bacterial suspension (2 µl) was added to each well and the cultures were incubated at 37 °C for 12 h. Samples were then washed twice with PBS to remove planktonic bacteria. Samples were stained using a Live/Dead BacLight Viability kit (Molecular Probes) that contained Syto 9 and propidium iodide. Samples were imaged using an inverted fluorescence microscope, where live bacteria fluoresced green and dead bacteria fluoresced red.

Two-photon fluorescence microscopy. For quantification of antibacterial activity, a home-built, two-photon fluorescence microscope was employed to image the samples stained with the Live/Dead BacLight Viability kits. The system included a mode-locked titanium–sapphire laser (MaiTai DeepSee eHP, Newport), which provided light at ~150 fs pulse width at a 80 MHz repetition rate. The emitted light was detected by two photomultiplier tubes through appropriate dichroic and bandpass filters for Syto9 and propidium iodide. A ×10, 0.3 numerical aperture objective (Leica) was used for visualization of multiple beads in one field-of-view (FOV; at ×10 this was approximately $600\times600\,\mu m^2$), while a ×40, 0.6 numerical aperture objective (Nikon) was used for quantification of live/dead bacteria fluorescence. At least five images were randomly selected across each sample for data quantification.

Antibacterial activity of RVPE on biofilm between the bone–titanium interface. RVPE was machined into discs (5 mm diameter). The following were also used: (1) a 4-mm-thick consolidated UHMWPE without additives (control), which was prepared using the same moulding conditions; (2) titanium discs coated on one side with titanium beads (10 mm diameter, 5 mm thickness, bead diameter 100 µm; manufactured by Orchid Orthopedics); and (3) bovine cortical bone discs (10 mm diameter, 3 mm thickness; the bovine cortical bone was machined from bovine tibia obtained from Animal Technology). All samples were sterilized with ethylene oxide gas. Fresh overnight liquid culture of bioluminescent *S. aureus* was diluted to $5\times10^4\,cfu\,ml^{-1}$ and 50 µl of the liquid culture was added on top of the beaded surface of the titanium discs to simulate an infection at an orthopaedic implant–bone interface. Cortical bone was added on top of the titanium disc seeded with bacteria and held together with a circular clamp (McMaster–Carr). The constructs were immersed in 5 ml of fresh Mueller–Hinton II broth and then incubated at 37 °C for 48 h. Then, the media was aspirated, clamps were removed, and titanium discs and cortical bone were separated and washed with PBS to remove planktonic bacteria. Biofilm formation was measured using a bioluminescence camera (IVIS 100, PerkinElmer). Cortical bone was placed back on top of the titanium after imaging and either control UHMWPE or RVPE were added underneath the titanium–bone constructs, then clamped using sterile clamps. Samples were placed in separate wells in a 6-well plate and 5 ml of Mueller–Hinton II broth was added to each well. All samples were incubated at 37 °C. Bioluminescence was measured at 24 h, 48 h, 96 h, 120 h, 1 week and 2 weeks after exposure to either the control or RVPE. During each bioluminescence measurement, the media was aspirated, clamps were removed, and the titanium discs and cortical bone were separated and washed with PBS to remove planktonic bacteria. The titanium discs and cortical bone were imaged separately. After imaging, the constructs were reassembled, new sterile clamps were used and new Mueller–Hinton II media was added. The media was replaced every 24 h. After the samples reached the predetermined time point, they were then stained using Live/Dead BacLight Viability kits that contained Syto 9 and propidium iodide. Samples were imaged using two-photon fluorescence microscopy. Percent red fluorescence, corresponding to percent cell death, was calculated using Matlab (r2015b; www.mathworks.com/products/matlab.html) by dividing the number of red pixels by the total number of fluorescent pixels.

Lapine planktonic bacteria PJI model. Study approval was granted from Pine Acres Research Facility Institutional Animal Care and Use Committee (protocol 15-06). Based on the pilot *in vivo* mouse study, the standard deviation in total flux from bioluminescence was $200{,}000\,p\,s^{-1}$. Taking type I error of 5% and 80% power to detect the mean difference of the total bioluminescent flux between the control and treatment groups of $370{,}000\,p\,s^{-1}$, a sample size of at least 4.6 was needed per group. In total, ten fully immune-competent, skeletally mature male New Zealand rabbits aged 12 months were used. Animals were randomly assigned to control (non-antibiotic-eluting UHMWPE) or VPE (7 wt% vancomycin-blended UHMWPE) groups. Each rabbit in the control group received two UHMWPE-only implants (3 mm diameter, 6 mm height) in the patellofemoral groove, and one beaded titanium rod in the tibial canal (4 mm diameter, 12 mm length). Each rabbit in the VPE group received two VPE implants (same dimensions as control) in the patellofemoral groove and one beaded titanium rod in the tibial canal (same dimensions as control).

Anaesthesia was achieved using intramuscular ketamine–xylazine ($40\,mg\,kg^{-1}$–$5\,mg\,kg^{-1}$) and inhaled isoflurane (1.5–2.5%) supplemented with oxygen ($1.2\,l\,min^{-1}$). Pre-emptive analgesia was administered 30 min before the procedure started (buprenorphine 0.02–0.05 $mg\,kg^{-1}$ subcutaneously (SC)). No pre- or post-operative antibiotics were administered. The rabbits were placed in the supine position and the right or left leg was prepped and draped in a sterile fashion (randomization of operated leg was established using www.random.org). A parapatellar incision was performed, the joint capsule was incised, the patella was displaced and two osteochondral defects were created in the trochlear groove (2.9 mm diameter, 6 mm depth). No antibiotic polyethylene (control branch) or VPE (VPE branches) implants were press-fitted into the defects. For the titanium implant, the tibial plateau was accessed and a defect was created by drilling distally into the marrow, creating a 3.9-mm-diameter and 12-mm-depth defect. Bioluminescent *S. aureus* (5×10^7 cfu in 50 µl 0.9% saline) was injected into the tibial defect, followed by press-fitting the titanium implant to seal the bacteria *in situ*. The patella was then relocated onto the trochlear groove and soft tissues were approximated using sutures. An additional dose of 5×10^7 cfu of bioluminescent *S. aureus* in 50 µl 0.9% saline was injected into the knee. All animals received buprenorphine 0.02–0.05 $mg\,kg^{-1}$ SC every 12 h throughout the study. After recovering from anaesthesia, rabbits were housed individually in cages (~55.8 cm × 63.5 cm × 66 cm). Load bearing on implants was allowed immediately after surgery, as no postoperative limiting motion device was utilized. Twice a day, rabbits were removed from their cages and placed in an open space to visually inspect the operated joint and gait. All animals were monitored at least twice throughout the study. Complete blood count and chemistry (vancomycin, creatinine, body urea nitrogen, alanine aminotransferase and alkaline phosphatase) were assessed before surgery and postoperatively on day 3, day 7, day 14 and day 21.

Postmortem bioluminescence imaging was performed on all operated knees (a midline incision was performed on the knee and the joint capsule was opened to expose the joint space). Bioluminescence signal was measured whenever the rabbits expired or when the study endpoint was reached (day 21). After imaging, the knees were dissected to aseptically isolate the femur, quadriceps tendon (including patella and patellar tendon), tibia, titanium and UHMWPE implants. The titanium rods were stained with BacLight Bacterial Live/Dead Stain and imaged using two-photon fluorescence microscopy to detect presence of live bacteria. The femur, quadriceps tendon, tibia and UHMWPE implants were separately sonicated in sterile saline; saline was then cultured in Mueller–Hinton II broth at 37 °C for 24 h to detect live bacteria.

Lapine biofilm bacteria PJI model. Ten rabbits were randomly assigned to control (non-antibiotic-eluting UHMWPE) or RVPE (layered 6.7 wt% vancomycin and 3.3 wt% rifampin in UHMWPE and non-antibiotic UHMWPE) groups. Each rabbit in the control group received two UHMWPE cylinders without additives (3 mm diameter, 6 mm length each) in the patellofemoral groove and one beaded titanium

rod covered with *S. aureus* biofilm in the tibial canal (4 mm diameter, 12 mm length). Each rabbit in the RVPE group received two RVPE implants (3 mm diameter, 6 mm length each) in the patellofemoral groove and one beaded titanium implant covered with *S. aureus* biofilm in the tibial canal (4 mm diameter, 12 mm length).

To create the *S. aureus* biofilm covered titanium rod, fresh overnight liquid culture of bioluminescent *S. aureus* was diluted to 5×10^4 cfu ml^{-1}. The liquid culture (50 µl) was added to 2 ml of Mueller–Hinton II broth. A sterile titanium rod was then immersed in the bacterial suspension and incubated at 37 °C for 48 h. Titanium rods were washed with PBS twice and then imaged with bioluminescent imaging to ensure uniform biofilm formation on all of the samples. One titanium rod was sacrificed for measurement of the biofilm thickness. The samples for use were then stained using a Live/Dead BacLight Viability kit that contained Cyto 9 and propidium iodide and imaged using two-photon fluorescence microscopy.

Anaesthesia was achieved using intramuscular ketamine-xylazine (40 mg kg^{-1}–5 mg kg^{-1}) and inhaled isoflurane (1.5–2.5%) supplemented with oxygen (1.2 l min^{-1}). Pre-emptive analgesia was administered before the procedure started (buprenorphine 0.02 mg kg^{-1}). No pre- or post-operative antibiotics were administered. The rabbits were placed in the supine position and the right or left leg was prepped and draped in a sterile fashion (randomization of operated leg established using www.random.org). A parapatellar incision was performed, the joint capsule was incised, the patella was displaced and two osteochondral defects were created in the trochlear groove (2.9 mm diameter, 6 mm depth). Control (for control branches) or VPE (for VPE branches) implants were press-fitted into the defects. For the titanium implant, the tibial plateau was accessed and a defect was created by drilling distally into the marrow, creating a 3.9-mm-diameter and 12-mm-depth defect. The biofilm-laden titanium implant was then press-fitted into the tibial canal. Load bearing on implants was allowed immediately after surgery, as no postoperative limiting motion device was utilized. Twice a day, rabbits were removed from their cages and placed in an open space to visually inspect the operated joint and gait. All animals were monitored at least twice per day for 3 days following surgery and at least once per day for the remainder of the study. Complete blood count and chemistry (vancomycin, creatinine, body urea nitrogen, alanine aminotransferase and alkaline phosphatase) were assessed before surgery and postoperatively on day 3, day 7, day 14 and day 21.

Postmortem bioluminescence imaging, tissues and implant sonication were performed as described in 'Lapine planktonic bacteria PJI model'.

Murine osseointegration model. Based on the pilot *in vivo* rat study, the standard deviation in BV/TV was 15%. Taking type I error of 5% and 80% power to detect a mean difference of BV/TV between the control and treatment groups of 23%, a sample size of at least four rats was needed per group. Eight Sprague–Dawley rats aged 8 weeks were randomly assigned into either control (non-antibiotic-eluting UHMWPE) or RVPE (layered 6.7 wt% vancomycin and 3.3 wt% rifampin in UHMWPE and non-antibiotic UHMWPE) groups. Each rat in the control group received an UHMWPE implant without antibiotics (3 mm diameter, and 4 mm length) transcondylarly in the medial distal femur and one stainless steel screw (3.5 mm diameter, 5 mm length) in the tibial canal between the intercondylar eminence.

Anaesthesia was achieved using inhaled isoflurane (1.5–2.5%) supplemented with oxygen (1.2 l min^{-1}). Pre-emptive analgesia was administered before the procedure started (buprenorphine 0.02 mg kg^{-1}). No pre- or post-operative antibiotics were administered. The rats were placed in the supine position and the right or left leg was prepped and draped in a sterile fashion (randomization of operated leg was established using www.random.org). A parapatellar incision was performed, the joint capsule was incised, the patella was displaced and a transcondylar defect on the medial distal femoral condyle was created. Control or RVPE implants were press-fitted into the defects. For the stainless steel screw implantation, the tibial plateau was accessed and a defect was created by drilling distally into the marrow canal. The biofilm-laden titanium implant was then screwed into the tibial canal. Load bearing on implants was allowed immediately after surgery, as no postoperative limiting motion device was utilized. Twice a day, rats were removed from their cages and placed in an open space to visually inspect the operated joint and gait. All animals were monitored at least twice per day for 3 days following surgery and at least once per day for the remainder of the study, up to 6 weeks.

After the rats were euthanized using CO_2, the operated femur and tibia were obtained and soft tissues were removed carefully. Each tibia was scanned with micro-CT to give 8 µm resolution in all three directions. 3D image reconstructions were generated using Avizo software (version 9.0; FEI). The BV/TV ratio was determined by creating a region of interest in the shape of a 3D cylinder (5 mm diameter, 3 mm height) along the long axis of the screw and centred on the long axis of the screw. A height of 3 mm was chosen as the thickness to allow quantification consistently on the epiphysis region. The same region of interest was used for all samples. The 3D images were thresholded to differentiate hard tissue (bone), screw and soft-tissue empty space. BV was calculated from the volume of the bone and TV was calculated as the total volume of bone and soft-tissue empty space.

Statistical analysis. Student's two-tailed *t*-tests were performed to compare two groups and analysis of variance (ANOVA) was performed for comparisons of multiple groups, through GraphPad Prism (version 4.0; www.graphpad.com); data reported denote the means ± s.d. of at least three independent experiments, except for that from the lapine study (single experiment). Survival analyses were performed using a log-rank test in GraphPad Prism; data reported denote the means ± s.d., combined from three independent experiments.

Data availability. The authors declare that all data supporting the findings of this study are available within the paper and its supplementary information.

Received 15 August 2016; accepted 2 May 2017; published 13 June 2017

References

1. *National Hospital Discharge Survey* 777–782 (Centers for Disease Control and Prevention/National Center for Health Statistics, 2010).
2. Paxton, E. W., Inacio, M., Slipchenko, T. & Fithian, D. C. The Kaiser Permanente National Total Joint Replacement Registry. *Perm. J.* **12,** 12–16 (2008).
3. *Hip and Knee Arthroplasty: Annual Report 2015* (Australian Orthopaedic Association National Joint Replacement Registry, 2015).
4. Kurtz, S. M., Lau, E., Watson, H., Schmier, J. K. & Parvizi, J. Economic burden of periprosthetic joint infection in the United States. *J. Arthroplasty* **27,** 61–65 (2012).
5. Kubista, B. *et al.* Reinfection after two-stage revision for periprosthetic infection of total knee arthroplasty. *Int. Orthop.* **36,** 65–71 (2012).
6. Lentino, J. R. Prosthetic joint infections: bane of orthopedists, challenge for infectious disease specialists. *Clin. Infect. Dis.* **36,** 1157–1161 (2003).
7. Segawa, H., Tsukuyama, D. T., Kyle, R. F., Becker, D. A. & Gustilo, R. B. Infection after total knee arthroplasty. A retrospective study of the treatment of eighty-one infections. *J. Bone Joint Surg. Am.* **81,** 1434–1445 (1999).
8. Spellberg, B. & Lipsky, B. A. Systemic antibiotic therapy for chronic osteomyelitis in adults. *Clin. Infect. Dis.* **54,** 393–407 (2012).
9. Pioletti, D. P. *et al.* Orthopedic implant used as drug delivery system: clinical situation and state of research. *Curr. Drug Deliv.* **5,** 59–63 (2008).
10. Duncan, C. P. & Masri, B. A. The role of antibiotic-loaded cement in the treatment of an infection after a hip replacement. *Instr. Course Lect.* **44,** 305–313 (1995).
11. Radin, S., Campbell, J. T., Ducheyne, P. & Cuckler, J. M. Calcium phosphate ceramic coatings as carriers of vancomycin. *Biomaterials* **18,** 777–782 (1997).
12. Lin, S. S. *et al.* Development of a biodegradable antibiotic delivery system. *Clin. Orthop. Relat. R.* **362,** 240–250 (1999).
13. Burnett, R. S., Kelly, M., Hanssen, A. D. & Barrack, R. L. Technique and timing of two-stage exchange for infection in TKA. *Clin. Orthop. Relat. R.* **464,** 164–178 (2007).
14. Jung, J., Schmid, N. V., Kelm, J., Schmitt, E. & Anagnostakos, K. Complications after spacer implantation in the treatment of hip joint infections. *Int. J. Med. Sci.* **6,** 265–273 (2009).
15. Kühn, K.-D. *Bone Cements: Up-to-Date Comparison of Physical and Chemical Properties of Commercial Materials* 89–93 (Springer, 2000).
16. Lee, C. *in The Well-Cemented Total Hip Arthroplasty: Theory and Practice* (eds Breusch, S. & Malchau, H.) 60–66 (Springer, 2005).
17. Cho, C. H. *et al.* Elasto-plastic contact analysis of fatigue wear behaviour of UHMWPE tibial components. *Japan. J. Clin. Biomech.* **23,** 373–379 (2002).
18. Korhonen, R. K., Kostinen, A., Konttinen, Y. T., Santavirta, S. S. & Lapallainen, R. The effect of geometry and abduction angle on the stresses in cemented UHMWPE acetabular cups – finite element simulations and experimental tests. *BioMed. Eng. Online* **4,** 32 (2005).
19. Lilikakis A & Sutcliffe, M. P. F. The effect of vancomycin addition to the compression strength of antibiotic-loaded bone cements. *Int. Orthop.* **33,** 815–819 (2009).
20. Meyer, J., Piller, G., Spiegel, C. A., Hetzel, S. & Squire, M. Vacuum-mixing significantly changes antibiotic elution characteristics of commercially available antibiotic-impregnated bone cements. *J. Bone Joint Surg. Am.* **93,** 2049–2056 (2011).
21. Thomes, B., Murray, P. & Bouchier-Hayes, D. Development of resistant strains of *Staphylococcus epidermidis* on gentamicin-loaded bone cement *in vivo*. *J. Bone Joint Surg. Br.* **84,** 758–760 (2002).
22. Xie, Z. *et al.* Gentamicin-loaded borate bioactive glass eradicates osteomyelitis due to *Escherichia coli* in a rabbit model. *Antimicrob. Agents Ch.* **57,** 3293–3298 (2013).
23. Fan, J. B., Huang, C., Jiang, L. & Wang, S. Nanoporous microspheres: from controllable synthesis to healthcare applications. *J. Mater. Chem. B.* **2013,** 2222–2235 (2013).

24. Bawa, R., Siegel, R., Marasca, B., Karel, M. & Langer, R. S. An explanation for the controlled release of macromolecules from polymers. *J. Control. Release* **1,** 259–267 (1985).
25. Guo, Q. H., Guo, S. & Wang, Z. M. Estimation of 5-fluorouracil-loaded ethylene-vinyl acetate stent coating based on percolation threshold. *Int. J. Pharm.* **333,** 95–102 (2007).
26. Yi, Y. B. & Sastry, A. M. Analytical approximation of the percolation threshold for overlapping ellipsoids of revolution. *Proc. R. Soc. Lond. A* **460,** 2353–2380 (2004).
27. Plumlee, K. P. & Schwartz, C. J. Development of porous UHMWPE morphologies for fixation of gel-based materials. *J. Appl. Poly. Sci.* **114,** 2555–2563 (2009).
28. Amin, T. J., Lamping, J. W., Hendriks, K. J. & McIff, T. E. Increasing the elution of vancomycin from high-dose antibiotic-loaded bone cement: a novel preparation technique. *J. Bone Joint Surg. Am.* **94,** 1946–1951 (2012).
29. Collier J. P. *et al.* Comparison of cross-linked polyethylene materials for orthopaedic applications. *Clin. Orthop. Relat. R.* **414,** 289–304 (2003).
30. Ertl, P., Rohde, B. & Selzer, P. Fast calculation of molecular polar surface area as a sum of fragment-based contributions and its application to the prediction of drug transport properties. *J. Med. Chem.* **43,** 3714–3717 (2000).
31. Laverty, G., Alkawareek, M. Y. & Gilmore, B. F. The *in vitro* susceptibility of biofilm forming medical device related pathogens to conventional antibiotics. *Dataset Papers Sci.* **2014,** 250694 (2014).
32. Goldman, M., Gronsky, R. & Pruitt, L. The influence of sterilization technique and ageing on the structure and morphology of medical-grade ultra-high molecular weight polyethylene. *J. Mater. Sci.-Mater. M.* **9,** 207–212 (1998).
33. Kurtz, A. & Patel, J. D. in *UHMWPE Biomaterials Handbook* 3rd edn (ed. Kurtz, S. M.) 57–71 (Elsevier, 2016).
34. Besemer D. C. *et al.* Evidence of vitamin E grafting to polyethylene. In *Orthopaedic Research Society 2013 Annual Meeting* Poster 1055 (Orthopaedic Research Society, 2013).
35. Cui, Q., Mihalko, W. M., Shields, J. S., Ries, M. & Saleh, K. J. Antibiotic-impregnated cement spacers for the treatment of infection associated with total hip or knee arthroplasty. *J. Bone Joint Surg. Am.* **89,** 871–882 (2007).
36. Mellor, J. A., Kingdom, J., Cafferkey, M. & Keane, C. T. Vancomycin toxicity: a prospective study. *J. Antimicrob. Chemoth.* **15,** 773–780 (1985).
37. Glaudemas, A. W. J. M., Galli, F., Pacilio, M. & Signore, A. Leukocyte and bacteria imaging in prosthetic joint infection. *Eur. Cell. Mater.* **25,** 61–77 (2013).
38. Rose, W. E. & Poppens, P. T. Impact of biofilm on the *in vitro* activity of vancomycin alone and in combination with tigecycline and rifampicin against *Staphylococcus aureus*. *J. Antimicrob. Chemoth.* **63,** 485–488 (2008).
39. Yee, Y. C., Kisslinger, B., Yu, V. L & Jin, D. J. A mechanism of rifamycin inhibition and resistance in *Pseudomonas aeruginosa*. *J. Antimicrob. Chemoth.* **38,** 133–137 (1996).
40. Bradley, J. S. & Scheld, W. M. The challenge of penicillin-resistant *Streptococcus pneumoniae* meningitis: current antibiotic therapy in the 1990s. *Clin. Infect. Dis.* **24** (Suppl. 2)**,** S213–S221 (1997).
41. Oral, E. *et al.* A surface cross-linked UHMWPE stabilized by vitamin E with low wear and high fatigue strength. *Biomaterials* **31,** 7051–7060 (2010).
42. Lauderdale, K. J., Malone, C. L., Boles, B. R., Morcuende, J. & Horswill, A. R. Biofilm dispersal of community-associated methicillin-resistant *Staphylococcus aureus* on orthopedic implant material. *J. Orthop. Res.* **28,** 55–61 (2010).
43. Isefuku, S., Joyner, C. J. & Simpson, A. H. Toxic effect of rifampicin on human osteoblast-like cells. *J. Orthop. Res.* **19,** 950–954 (2010).
44. Moses, M. A., Brem, H. & Langer, R. Advancing the field of drug delivery: taking aim at cancer. *Cancer Cell* **4,** 337–341 (2003).
45. Ambrose, C. G. *et al.* Effective treatment of osteomyelitis with biodegradable microspheres in a rabbit model. *Clin. Orthop. Relat. R.* **421,** 203–299 (2004).
46. Surdam, J. W., Licini, D. J., Baynes, N. T. & Arce, B. R. The use of exparel (liposomal bupivacaine) to manage postoperative pain in unilateral total knee arthroplasty patients. *J. Arthroplasty* **30,** 325–329 (2015).
47. Meyer, F. *et al.* Effects of lactic acid and glycolic acid on human osteoblasts: a way to understand PLGA involvement in PLGA/calcium phosphate composite failure. *J. Orthop. Res.* **30,** 864–871 (2012).
48. Bohner, M. in *Injectable Biomaterials: Science and Applications* (ed. Vernon, B.) 24–39 (Woodhead, 2011).
49. Hua, X. *et al.* Experimental validation of finite element modelling of a modular metal-on-polyethylene total hip replacement. *Proc. Inst. Mech. Eng. H* **228,** 682–692 (2014).
50. Neut, D. *et al.* Biomaterial-associated infection of gentamicin-loaded PMMA beads in orthopaedic revision surgery. *J. Antimicrob. Chemoth.* **47,** 885–891 (2001).
51. van de Belt, H. *et al. Staphylococcus aureus* biofilm formation on different gentamicin-loaded polymethylmethacrylate bone cements. *Biomaterials* **22,** 1607–1611 (2001).
52. Antoci, V. *et al.* Vancomycin covalently bonded to titanium alloy prevents bacterial colonization. *J. Orthop. Res.* **25,** 858–866 (2007).
53. Stewart, S. *et al.* Vancomycin-modified implant surface inhibits biofilm formation and supports bone-healing in an infected osteotomy model in sheep. *J. Bone Joint Surg. Am.* **94,** 1406–1415 (2012).
54. Castaneda, P., McLaren, A., Tavaziva, G. & Overstreet, D. Biofilm antimicrobial susceptibility increases with antimicrobial exposure time. *Clin. Orthop. Relat. R.* **474,** 1659–1664 (2016).
55. Xiong, Y. Q. *et al.* Real-time *in vivo* bioluminescent imaging for evaluating the efficacy of antibiotics in a rat *Staphylococcus aureus* endocarditis model. *Antimicrob. Agents Ch.* **49,** 380–387 (2005).
56. Kadurugamuw, J. L. *et al.* Rapid direct method for monitoring antibiotics in a mouse model of bacterial biofilm infection. *Antimicrob. Agents Ch.* **47,** 3130–3137 (2003).
57. Zhang, Q. *et al.* Acceleration of emergence of bacterial antibiotic resistance in connected microenvironments. *Science* **333,** 1764–1767 (2011).
58. Gullberg, E. *et al.* Selection of resistant bacteria at very low antibiotic concentrations. *PLoS Pathog.* **7,** e1002158 (2011).
59. Pardo-Alonso, S., Vicente, J., Solorzano, E., Rodriguez-Perez, M. A. & Lehmhus, D. Geometrical tortuosity 3D calculations in infiltrated aluminium cellular materials. *Proc. Mater. Sci.* **4,** 145–150 (2014).
60. Ortez, J. H. in *Manual of Antimicrobial Susceptibility Testing* (ed. Coyle M. B.) 39–52 (American Society for Microbiology, 2005).

Acknowledgements

We are grateful to G. Wojkiewicz and B. Tricot from the Center for Systems Biology, Massachusetts General Hospital (MGH) for their assistance with the bioluminescence imaging. This work was performed in part at the Center for Nanoscale Systems (CNS), a member of the National Nanotechnology Infrastructure Network (NNN), which is supported by the National Science Foundation (NSF) under NSF award no. ECS-0335765. The CNS is part of Harvard University. This study was supported in part by the Harris Orthopedics Lab Sundry Fund, MGH Orthopedics Departmental Fund, US National Institutes of Health grants P01-HL120839 and P41-EB015903.

Author contributions

V.J.S., D.A.B, E.O., O.K.M., H.R., A.A.F., H.M., S.J.J.K. and S.H.Y. designed the experiments. V.J.S., D.A.B. and S.J.J.K. performed the experiments. All authors were involved in the analyses and interpretation of the data. V.J.S., D.A.B., S.J.J.K., E.O. and O.K.M. wrote the paper, with the help of the co-authors.

Additional information

Supplementary information is available for this paper.

Reprints and permissions information is available at www.nature.com/reprints.

Correspondence and requests for materials should be addressed to E.O.

How to cite this article: Suhardi, V. J. *et al.* A fully functional drug-eluting joint implant. *Nat. Biomed. Eng.* **1,** 0080 (2017).

Publisher's note: Springer Nature remains neutral with regard to jurisdictional claims in published maps and institutional affiliations.

Competing interests

The authors declare no competing financial interests.